

Inventory of the Supplementary Information

- Figure S1. Full-length RidL and RidL-N, but not RidL-C, bind to PtdIns(3)P.
- Figure S2. Cellular localization of RidL-FL, RidL-N, and RidL-C.
- Figure S3. Stereo view of RidL loop with a composite Simulated Annealing omit map at 2.5 Å resolution and contoured at 1σ .
- Figure S4. Sequence comparison of RidL from different *Legionella* species.
- Figure S5. Identification and characterization of PtdIns(3)P binding residues in RidL-N.
- Figure S6. VARP and TBC1d5 recognize VPS29 through similar modes.
- Figure S7. Interaction between TBC1d5 and VPS29 proteins.
- Table S1. Crystallography Data Collection and Refinement Statistics.
- Table S2. DNA Constructs Used in this Study.
- Table S3. Summary of Antibodies Used in this Study

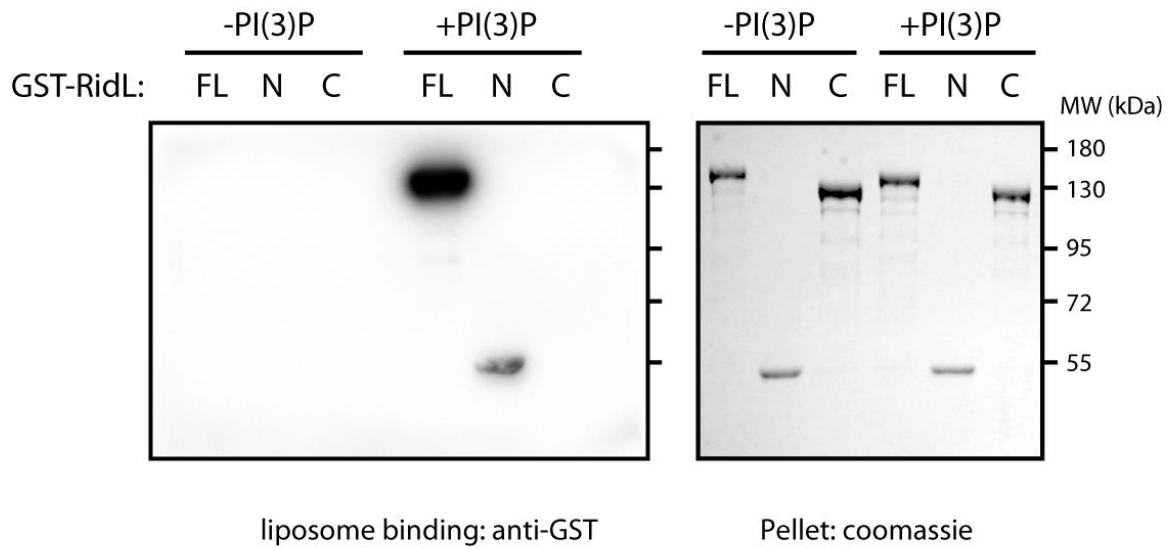


Figure S1

Figure S1. Full-length RidL and RidL-N, but not RidL-C, bind to PtdIns(3)P.

Left: Proteins associated with PtdIns(3)P-containing or PtdIns(3)P-free liposomes were immunoblotted with anti-GST antibody. Right: GST-fusion proteins in pellet stained by coomassie blue.

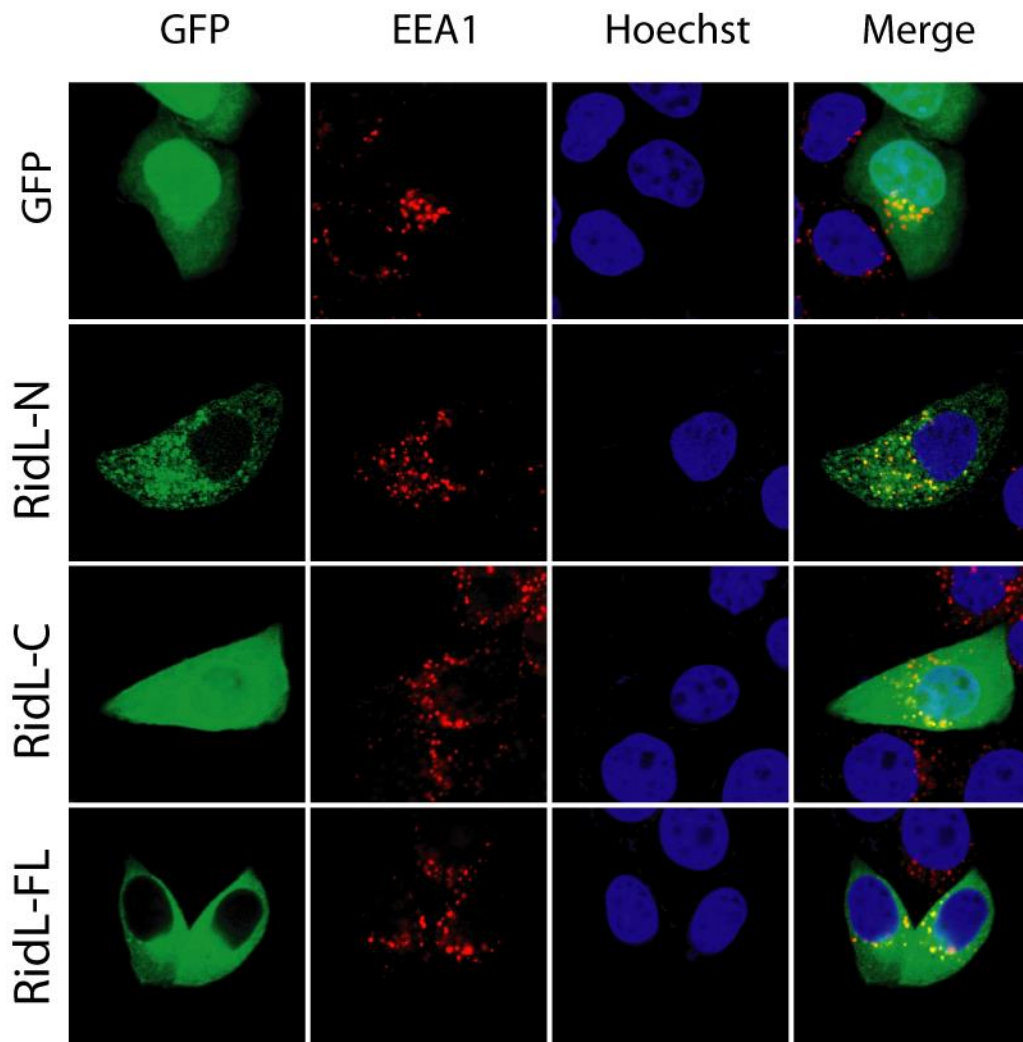


Figure S2

Figure S2. Cellular localization of RidL-FL, RidL-N, and RidL-C. HeLa cells were transfected with GFP, or GFP-RidL-FL, RidL-N, RidL-C (green), and then fixed and labeled with anti-EEA1 (red) antibody.

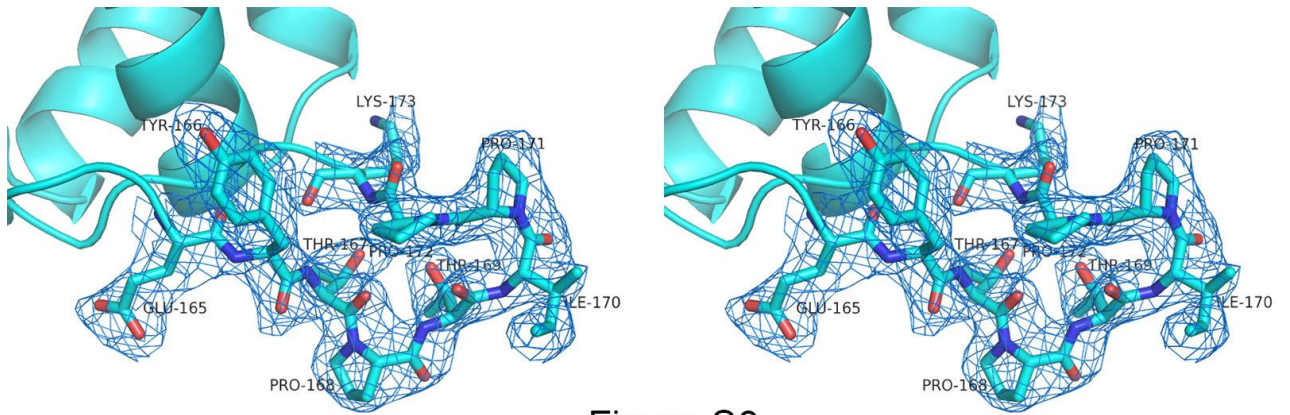


Figure S3

Figure S3. Stereo view of the RidL loop with a composite Simulated Annealing omit map at 2.5 Å resolution and contoured at 1σ .

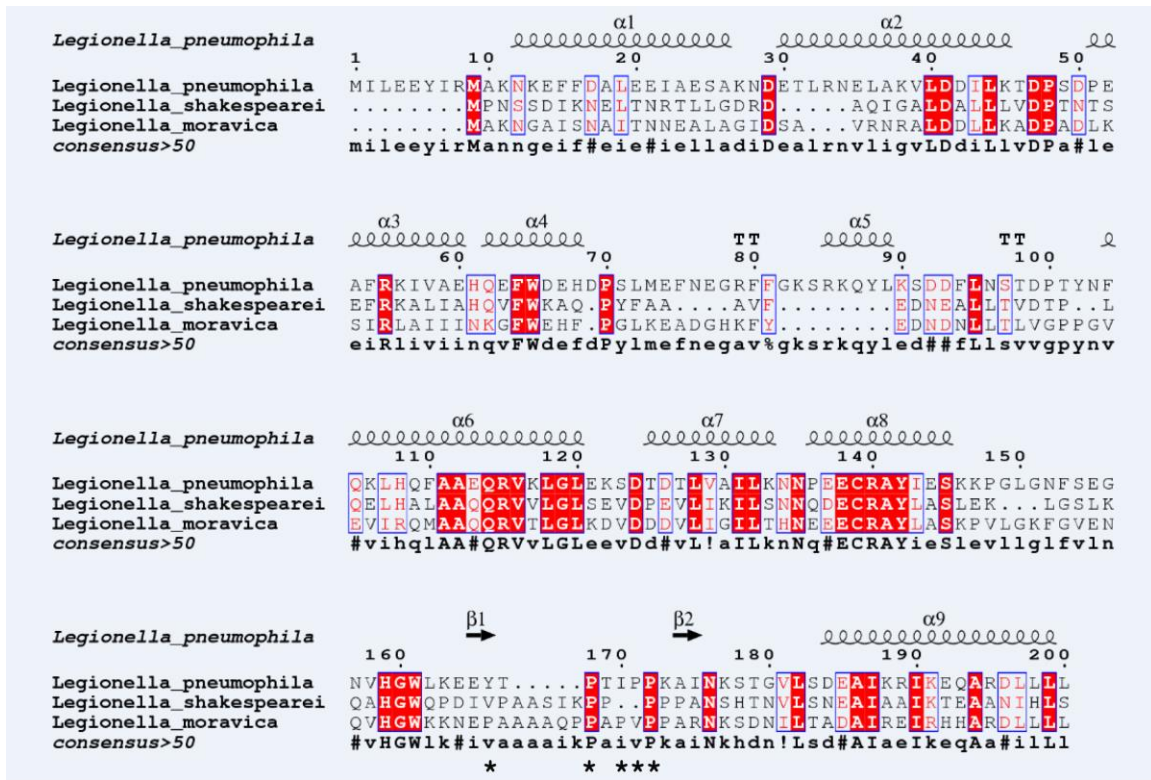


Figure S4

Figure S4. Sequence comparison of RidL from different *Legionella* species. *L. moravica* or *L. shakspareii* RidL proteins are the two closest homologs to *L. pneumophila* RidL. Sequence alignments were performed with ClustalW, with protein secondary structure listed above and consensus sequence listed below. The residues that interact with VPS29 are labeled with a “*” at the bottom of alignment.

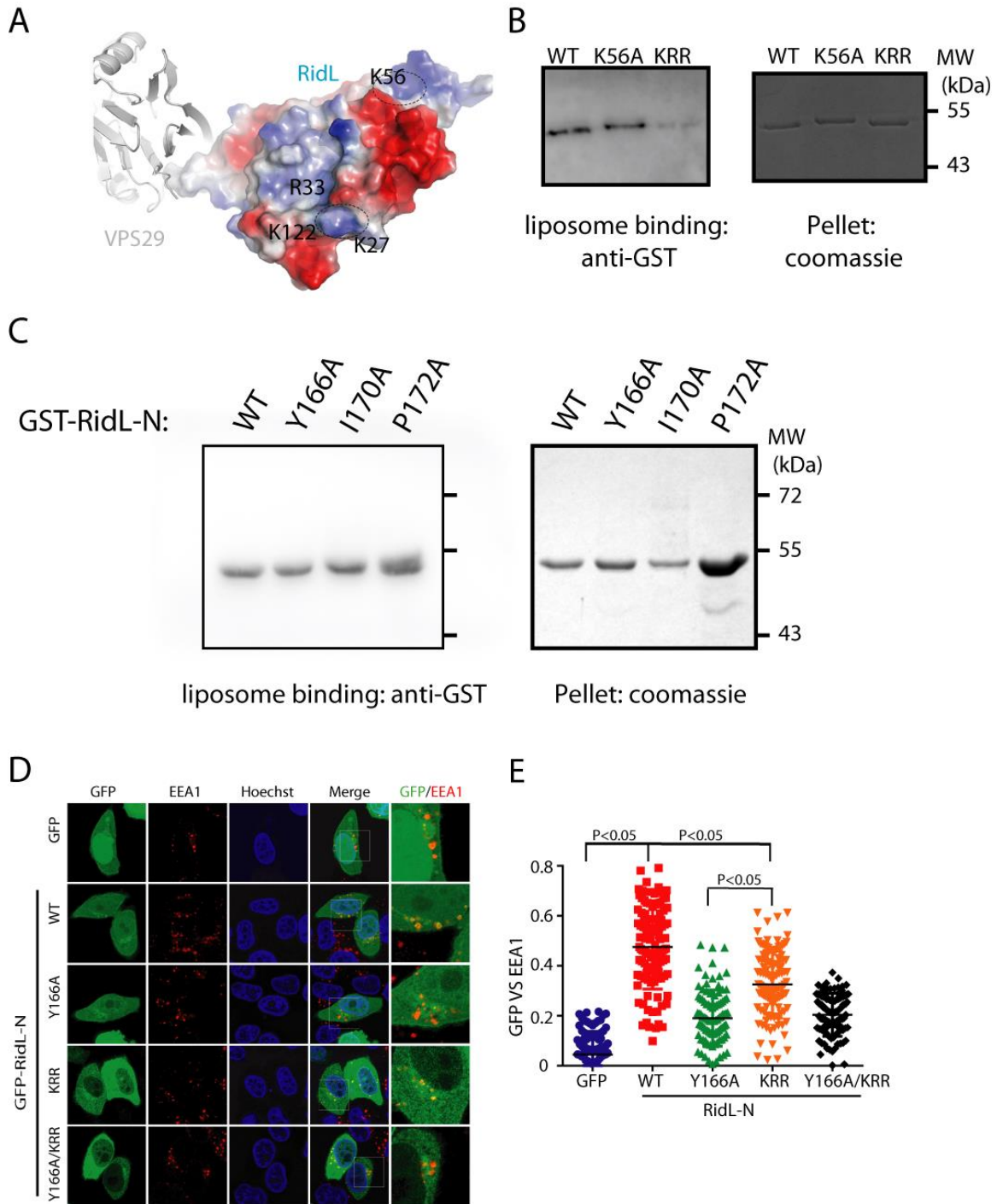


Figure S5

Figure S5. Identification and characterization of PtdIns(3)P binding residues in RidL-N.

(A) VPS29-RidL complex structure highlighting two positively charged surfaces (circled) on RidL that are distant from the VPS29-binding site.

(B) PtdIns(3)P-containing liposome flotation assay. Left: liposome-bound samples were probed with anti-GST antibody; right: GST-fusion proteins in pellet stained by coomassie blue.

(C) VPS29-interacting deficient RidL mutants binds to PtdIns(3)P-containing liposome similar to RidL WT. Left: liposome-bound samples were probed with anti-GST antibody; right: GST-fusion proteins in pellet stained by coomassie blue.

(D) HeLa cells were transfected with GFP, or GFP-RidL-N WT, Y166A, KRR, Y166A/KRR (green), and then fixed and labeled with anti-EEA1 (red) antibody.

(E) Quantitation of GFP colocalization with EEA1 in cells in (c). Each dot represents Pearson's correlation coefficients from one cell. P values shown are the result of one-way ANOVA, post hoc Tukey's test.

A

```
Human_TBC1d5 132 GQQDLMINNPLSQDEGSLWNKFFQDKE 158
Human_VARP   424 KDTVQKMCHPLCFCDDCEKLVSGRLND 450
Human_VARP   704 SAADEFECHPLCQCPKCAPAQKRLAKV 730
```

B

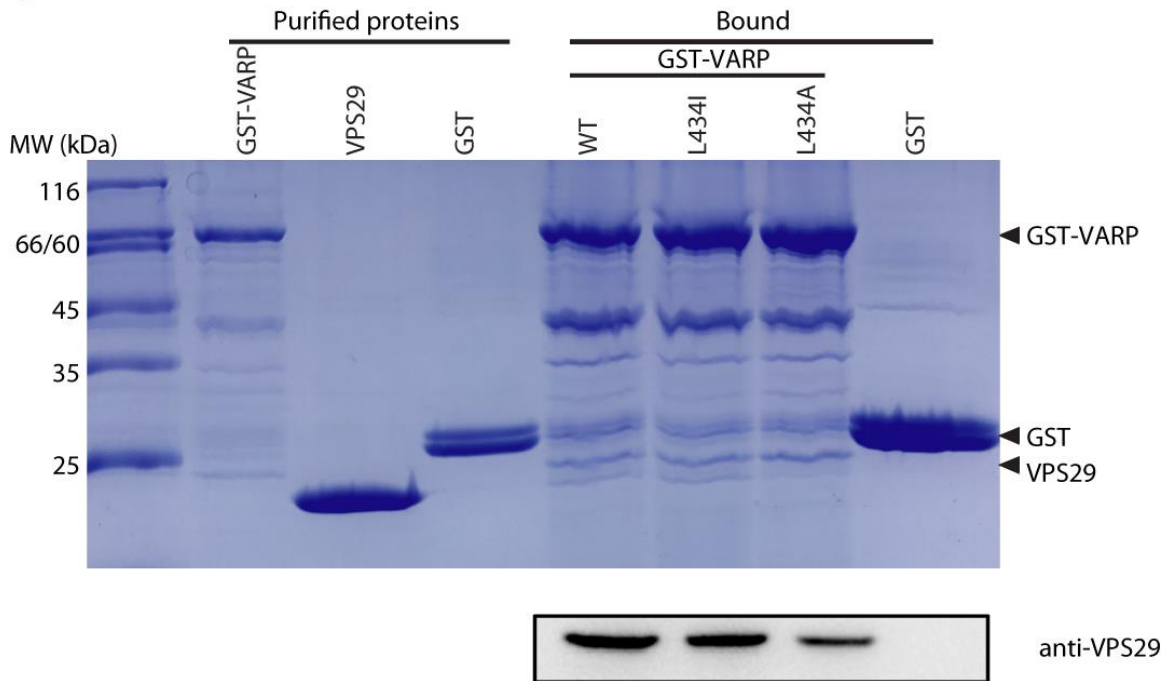


Figure S6

Figure S6. VARP and TBC1d5 recognize VPS29 through similar modes.

(A) Sequence comparison of Ins1 of TBC1d5 and two cysteine-rich motifs of VARP.

Conserved residues are highlighted in machaccino. The leucine residue mutated in the pull-down experiment in (B) is labeled with a black triangles on top.

(B) GST-VARP (aa1-450) WT, mutants or GST pull-down of purified VPS29. Shown are a coomassie blue stained SDS-PAGE gel of purified proeins and bound samples (top),

and immunoblot using anti-VPS29 antibody for the same sample (bottom). The GST-VARP samples contained multiple degraded proteins whose sizes range from that of GST-VARP to that of GST.

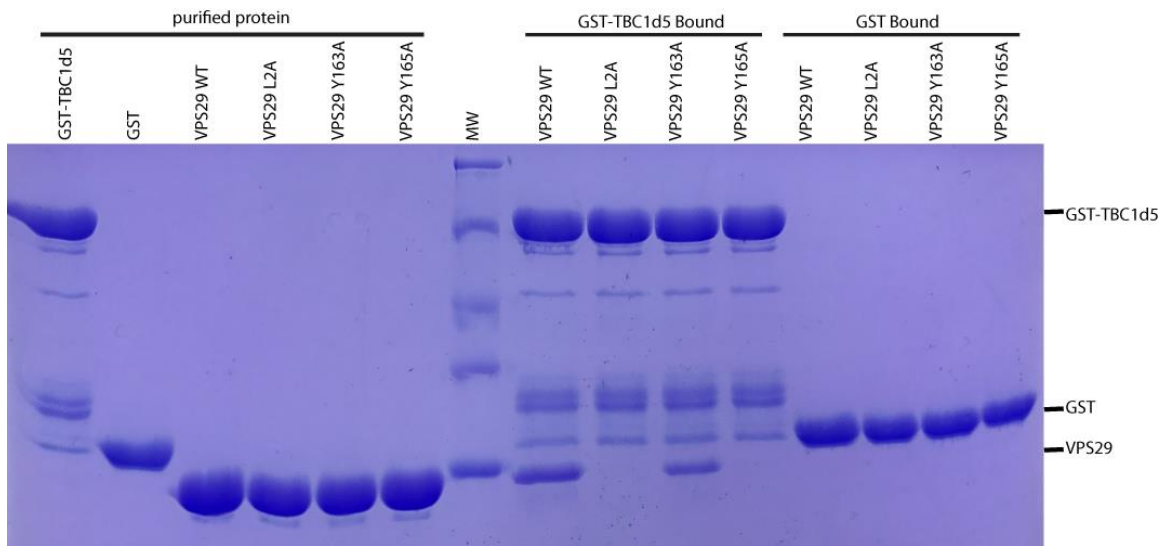


Figure S7

Figure S7. Interaction between TBC1d5 and VPS29 proteins.

GST-TBC1d5 (aa1-419) or GST pull-down of purified VPS29 WT or mutants. Shown are a coomassie blue stained SDS-PAGE gel of purified proteins and bound samples (top).

Table S1. Crystallography Data Collection and Refinement Statistics.

	<i>VPS29:RidL</i> ⁵⁻²⁰⁵
Cell axial lengths (Å)	$a=44.31, b=82.05, c=87.33$ $\alpha=101.73, \beta=104.26, \gamma=104.77$
Spacegroup	P ₁
Data collection	
Resolution range (Å)	50.00-2.50 (2.54-2.50)
Number of observed reflections	139107 (6728)
Number of unique reflections	36022 (1764)
Completeness (%)	96.7 (97.0)
Redundancy	3.7 (3.7)
Rmerge	0.106 (0.891)
Highest shell CC1/2	0.722
Mean I/I_{σ}	14.4 (1.9)
Solvent content (%)	62.6
Refinement	
Resolution range (Å)	50.00-2.50 (2.57-2.50)
Number of working reflections	30261 (405)
Number of test reflections	1602 (23)
R _{work} ^a (no. of reflections)	0.188 (0.232)
R _{free} ^b (no. of reflections)	0.224 (0.326)
R.m.s. deviation bond lengths (Å)	0.010
R.m.s. deviation bond angles (°)	1.406
Average B-factors (Å²) (# of atoms)	
VPS29 atoms	47.5 (2938)
RidL atoms	60.9 (3209)
Waters atoms	43.1 (226)
Ramachandran plot	
Most favored regions (%)	90.3
Allowed regions (%)	8.8
General allowed regions (%)	0.3
Disallowed regions (%)	0.6

R_{work}^b = $\sum |F_o - F_c| / |F_o|$, where F_c and F_o are the calculated and observed structure factor amplitudes, respectively
R_{free}^c calculated as for R_{work} but for 5.0% of the total reflections chosen at random and omitted from refinement for all data sets
values in the parenthesis is information from highest resolution shell.

Table S2. DNA Constructs Used in this Study.

Construct name	Source or reference
pEGFP-C1	Clontech #6084-1
pEGFP-C1-RidL	This paper
pEGFP-C1-RidL-N (aa1-200)	This paper
pEGFP-C1-RidL-N-Y166A	This paper
pEGFP-C1-RidL-N- I170A	This paper
pEGFP-C1-RidL-N-P172A	This paper
pEGFP-C1-RidL-C (aa201-C)	This paper
pEGFP-C1-RidL-N-KRR	This paper
pEGFP-C1-RidL-N-Y166A/KRR	This paper
pGEX-4T-1-RidL	This paper
pGEX-4T-1-RidL-N (aa1-200)	This paper
pGEX-4T-1-RidL-C (aa201-C)	This paper
pGEX-4T-1-RidL-N Y166A	This paper
pGEX-4T-1-RidL-N P168A	This paper
pGEX-4T-1-RidL-N I170A	This paper
pGEX-4T-1-RidL-N I170E	This paper
pGEX-4T-1-RidL-N I170L	This paper
pGEX-4T-1-RidL-N I170W	This paper
pGEX-4T-1-RidL-N P171A	This paper
pGEX-4T-1-RidL-N P172A	This paper
pGEX-4T-1-RidL-N-NKS (N176L/K177D/S178A)	This paper
pGEX-4T-1-loop ^{LP} (aa160-180)	This paper
pGEX-4T-1-RidL ^{LM}	This paper
pGEX-4T-1-RidL ^{LS}	This paper
pGEX-4T-1-RidL ^{LS} -loop ^{LP}	This paper

pCDF-1b-VPS29	(Jia et al., 2012)
pCDF-1b-VPS29 L2A	This paper
pCDF-1b-VPS29 L25A	This paper
pCDF-1b-VPS29 K30A	This paper
pCDF-1b-VPS29 Y163A	This paper
pCDF-1b-VPS29 Y165A	This paper
pCDF-1b-VPS29 R176A	This paper
pCDF-1b-VPS29 K56A	This paper
pCDF-1b-VPS29 KKR (K27A/R33A/K122A)	This paper
pGEX-4T-1-VPS35	(Jia et al., 2012)
pCDF-1b-VPS26	(Jia et al., 2012)
pGEX-4T-1-TBC1D5	(Jia et al., 2016)
pGEX-4T-1-VARP (aa1-450)	(Hesketh et al., 2014) ; this paper
pGEX-4T-1-VARP-L434I	This paper
pGEX-4T-1-VARP-L434A	This paper
pSTxB	(Liu et al., 2012)

Table S3. Summary of Antibodies Used in this Study

Antibody	SOURCE	Catalog #
VPS35	Gift from Dr. Dan Billadeau; (Jia et al., 2016)	N/A
VPS29	GeneTex	GTX104768
EEA1	BD Biosciences	610457
TBC1D5	PTG	17078-1-ap
TGN46	abcam	ab50595
STxB	Gift from Dr. Guihua Tai; (Liu et al., 2012)	N/A
GST	PTG	66001-1-Ig
Goat anti-rabbit IgG-HRP	Santa Cruz	sc-2004
TRITC affininipure goat anti-mouse IgG	Jackson ImmunoResearch	115-025-003
TRITC affininipure goat anti-rabbit IgG	Jackson ImmunoResearch	111-025-003
Alexa Fluor 647 affininipure goat anti-rabbit IgG	Jackson ImmunoResearch	111-605-003